Enhanced discrimination of boreal forest covers with directional reflectances from the airborne polarization and directionality of Earth reflectances (POLDER) instrument

P. Bicheron, M. Leroy, O. Hautecoeur, F.M. Bréon

JOURNAL OF GEOPHYSICAL RESEARCH, VOL. 102, NO. D24, PAGES 29,517–29,528, DECEMBER 26, 1997

Enhanced discrimination of boreal forest covers with directional reflectances from the airborne polarization and directionality of Earth reflectances (POLDER) instrument

P. Bicheron, M. Leroy, and O. Hautecoeur

Centre d'Etudes Spatiales de la Biosphère, Unité Mixte de Recherches, Centre National d'Etudes Spatiales, Centre National de la Recherche Scientifique, Université Paul Sabatier, Toulouse, France

F. M. Bréon

Laboratoire de Modélisation du Climat et de l'Environnement, Commissariat à l'Energie Atomique Direction des Sciences de la Matière/LMCE, Gif sur Yvette, France

Abstract. During the Boreal Ecosystem-Atmosphere Study (BOREAS), directional and spectral reflectance measurements were acquired from May to July 1994 with the polarization and directionality of Earth reflectances (POLDER) instrument on board a NASA C-130 aircraft. The instrument has a wide field-of-view optics, a two-dimensional CCD array, and a rotating wheel carrying filters in the visible and near infrared. Measurements were obtained (1) over coniferous forests at the young and old jack pine and old black spruce sites, (2) over a deciduous forest at the old aspen site, and (3) over a fen at the fen site. A prominent hot spot feature was apparent at each site, with an additional strong peak in the specular direction for the fen site. Strong variations of the bidirectional reflectance distribution function (BRDF) with sun zenith angle were observed. For a constant sun zenith angle, the variation of the BRDF of conifer stands between May and July was relatively weak. A key objective of this paper is to quantify the improvement of discrimination of various forest covers when remotely sensed directional signatures are added to the more conventional spectral signatures. The experimental protocol consisted of the following steps. First, 150 pixels pertaining to five different classes of forest covers were selected on land cover maps available in the BOREAS Information System (BORIS) data base. Second, the BRDF measurements acquired by POLDER at each pixel were adjusted against a three-parameter semiempirical BRDF model and processed to retrieve the reflectance seen in three different viewing directions. Third, the results of supervised classifications were compared on all selected pixels, using as input, either the reflectances in only one direction (this simulates the case of conventional spectral signatures), or reflectances acquired in three directions (this simulates the case of spectral + directional signatures). The results showed that when only one spectral band was used, the proportion of correctly classified pixels increased from 36–59% with one viewing direction to 64–84% with three viewing directions. When three spectral bands were considered, this proportion improved from 72–87% to 83–97%. These results demonstrate that the account of directional information enhances the ability to discriminate forest covers by remote sensing.

1. Introduction

Remote sensing observations of the surface reflectance anisotropy have received increasing attention in recent years. Anisotropic effects have been evaluated using times series of the advanced very high resolution radiometer (AVHRR), for which the viewing zenith angle is highly variable in successive observations [*Gutman*, 1987; *Roujean et al.*, 1992; *Rahman et al.*, 1993; *Leroy and Roujean*, 1994; *Wu et al.*, 1995]. Such measurements have also been made in the field over bare soils, agricultural crops, or natural grasslands [*Ranson et al.*, 1986; *Kimes*, 1983; *Kuusk*, 1991]. Directional signatures of forests are inherently more difficult to measure because of the size of forests. They can be measured from high towers [*Deering et al.*, 1994] or from aircraft or helicopter [*Kimes et al.*, 1986; *Kleman*, 1987; *Syrén*, 1994] using the advanced solid-state array spectroradiometer (ASAS) instrument [*Irons et al.*, 1991; *Schaaf and Strahler*, 1994; *Russell et al.*, 1995] and the polarization and directionality of Earth's reflectances (POLDER) instrument [*Deschamps et al.*, 1994; *Leroy and Bréon*, 1996; *Bréon et al.*, 1997].

Land cover classification is an important application of remote sensing observations of natural surfaces. Much work has been done to classify vegetation types on a variety of scales, ranging from global or regional with NOAA-AVHRR data [*Tucker et al.*, 1985; *Sellers et al.*, 1994; *Achard and Estreguil*, 1995], to local with high-resolution sensors such as Landsat or SPOT [*Morton*, 1986; *Walker et al.*, 1986; *Singh*, 1987]. Although temporal information is sometimes used in classifications, as done by *Townshend et al.* [1987], most classifications only use the spectral information content of reflectances. The

Paper number 97JD01330.
0148-0227/97/97JD-01330$09.00

Table 1. List of Airborne POLDER/C-130 Data Acquisitions

Site	Latitude, deg N	Longitude, deg W	Date	Sun Zenith Angle, deg	Aerosol Thickness at 550 nm	
					Total	Below
Fen	53.799	104.62	July 24	44.4–49.3	0.080	0.020
Old jack pine	53.916	104.69	May 31	38.4–42.8	0.130	0.055
			June 1	48.4–51.4	0.095	0.050
			July 21	33.8–35.0	0.120	0.095
			July 24	40.5–43.3	0.095	0.020
Old aspen	53.629	106.20	May 26	39.4–41.8	0.115	0.075
			May 31	46.5–52.5	0.070	0.025
Young jack pine	53.875	104.65	June 1	44.0–47.0	0.095	0.050
			July 21	35.5–37.2	0.115	0.090
Old black spruce	53.985	105.12	May 31	35.5–37.4	0.135	0.070
			June 1	53.5–56.4	0.060	0.030
			July 21	33.4–33.7	0.115	0.090

To each site flown over is associated its latitude and longitude, range of Sun angles during overpass, and aerosol optical thickness at 550 nm, total and below the plane.

potential of directional information to classify cover types has been suggested in the past [*Goel and Reynolds*, 1989] but has only recently begun to be evaluated quantitatively [*Abuelgasim et al.*, 1996; *Hyman and Barnsley*, 1997].

The first objective of this paper is to document measurements of the spectral and directional reflectances of various boreal forest covers of the southern study area of the Boreal Ecosystem-Atmosphere Study (BOREAS) experiment. Reflectances were acquired by the POLDER instrument on board a C-130 airplane operated by NASA Ames Research Center during the first two Intensive Field Campaigns (IFC 1 and IFC 2) from May to July 1994. The second objective is to quantify the improvement of classifications of boreal cover types when the directional signature is used in addition to the more conventional spectral signature. This study made use of the capabilities of the POLDER instrumental concept to derive directional measurements on a large number of different surface targets in extended areas [*Leroy and Bréon*, 1996].

2. The POLDER Instrument

The POLDER instrument [*Deschamps et al.*, 1994] is a radiometer designed to measure the directionality and polarization of the sunlight scattered by the ground-atmosphere system. The instrument generates bidimensional images of the surface on a CCD array (288 × 384 pixels) through a wide field of view optics. A given pixel may be observed under different viewing angles in consecutive images acquired along the flight lines. The airborne instrument has an angular coverage of ±43° in the cross-track direction and ±51° in the along-track direction. The ground pixel size is proportional to the instrument altitude. It is 35 m × 35 m at an altitude of 5500 m, the height generally flown by the C-130 during the BOREAS experiment. A rotating filter wheel which carries spectral filters and polarizers oriented by steps of 60° allows measurements in several spectral bands centered on 443 nm (three directions of polarization), 550, 670, 864 (three directions of polarization), and 910 nm. The bandwidth is 10–20 nm, depending on the band. The first filter wheel position yields dark current measurements. A sequence of 10 images, corresponding to the 10 positions of the filter wheel, is performed within 3 s and is repeated every 10 s. The processing of successive images permits the reconstruction of the bidirectional reflectance distribution function (BRDF) for each pixel. For a typical C-130 flight altitude and speed, an angular resolution of approximately 8° is achieved along-track.

3. Data Acquisition and Processing

Flights over tower sites of the south study area in both IFC 1 and IFC 2 campaigns are summarized in Table 1. The overflown tower sites were the fen (one date), old jack pine (four dates), old aspen (two dates), young jack pine (two dates), and old black spruce (three dates). Only spectral bands centered on 550, 670, and 864 nm are considered in this study. Each target was overflown several times, each time at a different heading, in the principal solar plane, and at planes perpendicular and oblique to that plane. For each image acquisition, POLDER recorded the aircraft position and attitude. The bias between the C-130 inertial reference system and the POLDER optical axis were measured before each flight. These parameters should, in principle, be sufficient to geometrically correct POLDER images. However, the aircraft position given by the inertial reference system had a too large uncertainty, so ground control point techniques were used to fine-tune the geometric multi-image registration. Two techniques were applied, depending on the application. One such application was to derive the BRDF over tower sites. For this purpose, a single ground control point close to the target was used, and a translational correction was made on the geocoded image. These reflectance measurements were then spatially averaged on a 5 × 5 pixel (175 m × 175 m) window, around each tower site, to minimize residual misregistration effects. Another application was to generate BRDF data sets for each surface pixel over an area of size 5 km × 5 km with a spatial resolution of 100 m. Typically, 10 ground control points were used for each image. This approach was applied to the young jack pine and old black spruce data sets acquired on July 21.

Calibrations of the POLDER instrument were made with an integrating sphere before and after the BOREAS experiment on May 11 and October 24, 1994, respectively at Laboratoire d'Optique Atmosphérique (LOA) of Lille. Other calibration experiments took place in the field, on May 27 and July 21, 1994, using a 30-inch-diameter portable hemisphere operated

Table 2. Comparison of Absolute Calibration Coefficients Derived at Different Dates, at Laboratoire d'Optique Atmosphérique (LOA) Before and After the Experiment, and in the Field During the Experiment

	Wavelength, nm								
	443			550	670	864			910
	F1	F2	F3	F4	F5	F6	F7	F8	F9
LOA									
May 11	54.5	53.5	54.8	51.4	56.8	50.8	46.6	49.4	41.9
Oct. 12	59.0	57.9	59.1	53.2	58.8	53.7	49.3	52.1	44.0
Field									
May 27	56.3	55.1	56.1	50.2	55.0	50.2	45.8	48.6	44.5
July 21	67.7	66.4	67.7	56.9	61.3	55.7	51.0	53.8	47.8
Mean									
LOA	56.8	55.7	57.0	51.9	57.8	52.2	48.0	50.7	42.9
Field	62.0	60.8	61.8	53.5	58.1	52.9	48.4	51.2	46.1

Values are expressed in digital number outputs for a "normalized radiance" of 1% (input radiance multiplied by π divided by the exoatmospheric solar spectral irradiance).

by NASA Goddard Space Flight Center [*Markham et al.*, 1995]. This source could be positioned directly under the aircraft-mounted instrument. A correction for CCD temperature effects on the detector sensitivity was taken into account. The resulting absolute calibration coefficients are shown in Table 2. The two LOA experiments and the first field experiment are in good agreement (Table 2). The average-peak discrepancies within these three experiments are of the order of 3–5%, depending on the band. The second field calibration (July 21) shows an unexplained rise of instrumental sensitivity with respect to the former group of calibrations, of the order of 10–20%. Subsequent processing was made using the average calibration results obtained at LOA. Images were corrected for dark current and for CCD detector equalization coefficients calibrated at LOA. The resulting digital numbers were converted to radiances using the calibration coefficients, and then to reflectances by multiplying radiances by $\pi/E \cos \theta_s$, where E is the exoatmospheric solar irradiance and θ_s is the Sun zenith angle. For the polarized channels (443 and 864 nm), the reported reflectance is the average of the three reflectances measured for each polarizer.

The atmospheric correction algorithm 6S [*Vermote et al.*, 1997] was applied to the measured reflectances over tower sites to derive reflectances corrected for atmospheric effects. A midarctic summer atmospheric model and a continental aerosol model were selected to characterize the atmosphere above the BOREAS sites. Moreover, the total aerosol optical depth for the full atmosphere and the below-aircraft aerosol optical depth, both at 550 nm, were obtained from the BORIS database. Aerosol optical depths are given in Table 1 for each date and site overflown. All flight days of IFC 1 and IFC 2 were very clear, with an average value of the total aerosol optical depth of 0.10 at 550 nm. Assumptions made in the atmospheric correction (Lambertian surface reflectance, choice of the aerosol model) may induce errors in the procedure. These errors, however, are not expected to modify greatly the magnitude and shape of the resulting BRDF.

4. Angular and Spectral Signatures of Various Boreal Covers

The bidirectional spectral reflectances, corrected for atmospheric effects and averaged on 175 m × 175 m, are presented in Figures 1–4 for four different tower sites, old aspen (May 26), old black spruce and old jack pine (May 31), and fen (July 24) at 550, 670, and 864 nm. The radius of the polar diagrams represents the viewing zenith angle θ_v, and the polar angle is the relative azimuth ϕ between view and Sun direction. The aligned data points correspond to successive reflectance measurements (in percents) of a given flight line, which in general, belongs to the principal, perpendicular, or $\phi = 45°$ oblique plane of the tower site. The lines are a result of isocontour processing on the data points.

Visual analysis of the data plots gave confidence in the data quality. The measurements along a flight axis had a smooth aspect with a small high-frequency component. The points in the perpendicular plane were reasonably symmetric with respect to the principal plane. Such symmetry is expected if the target has no favored direction. Moreover, there was a rather good agreement between measurements for similar viewing directions acquired during different flight lines. Some of the differences could be attributed to variations in solar zenith angles between the beginning and the end of the site overflight.

The general pattern of the three data sets of forest signatures (Figures 1–3) was similar at all wavelengths. The measurements showed an important gradient in the principal plane and only small variations in the perpendicular plane. The maximum reflectance was systematically found in the so-called "hot spot" direction, where the viewing direction approaches the solar direction (in Figures 1–3 the minimum angle between Sun and view directions equals 2° for old aspen, 6° for old black spruce, and 3° for old jack pine). As discussed by *Bréon et al.* [1997], and confirmed by our data, the POLDER instrument allows the measurement of the hot spot phenomenon. The minimum reflectance was observed in the forward scatter direction.

Nevertheless, the reflectance magnitude depended on species. Since the solar zenith angles in Figures 1–3 were rather similar (about 40°), a comparison between different species was done. Thus values of 6.6% at 550 nm and 25.1% at 864 nm were observed for the old aspen site at nadir, contrasted with 5% at 550 nm and 18% at 864 nm for both the old black spruce and old jack pine sites. Furthermore, the ratio of maximum to minimum reflectances varied both with species and wavelength. For the conifer stands it was about 4 at 550 nm, 8 at

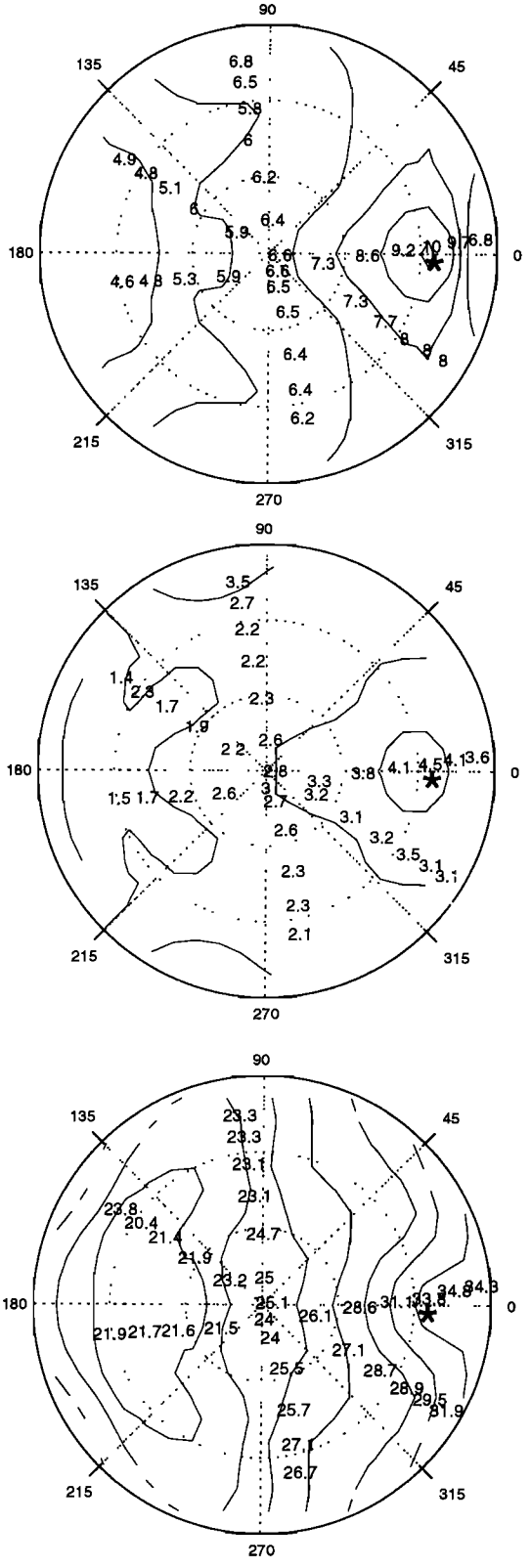

Figure 1. Directional and spectral diagram for the old aspen site on May 26, at 550 nm (top), 670 nm (middle), and 864 nm (bottom), corrected for atmospheric effects.

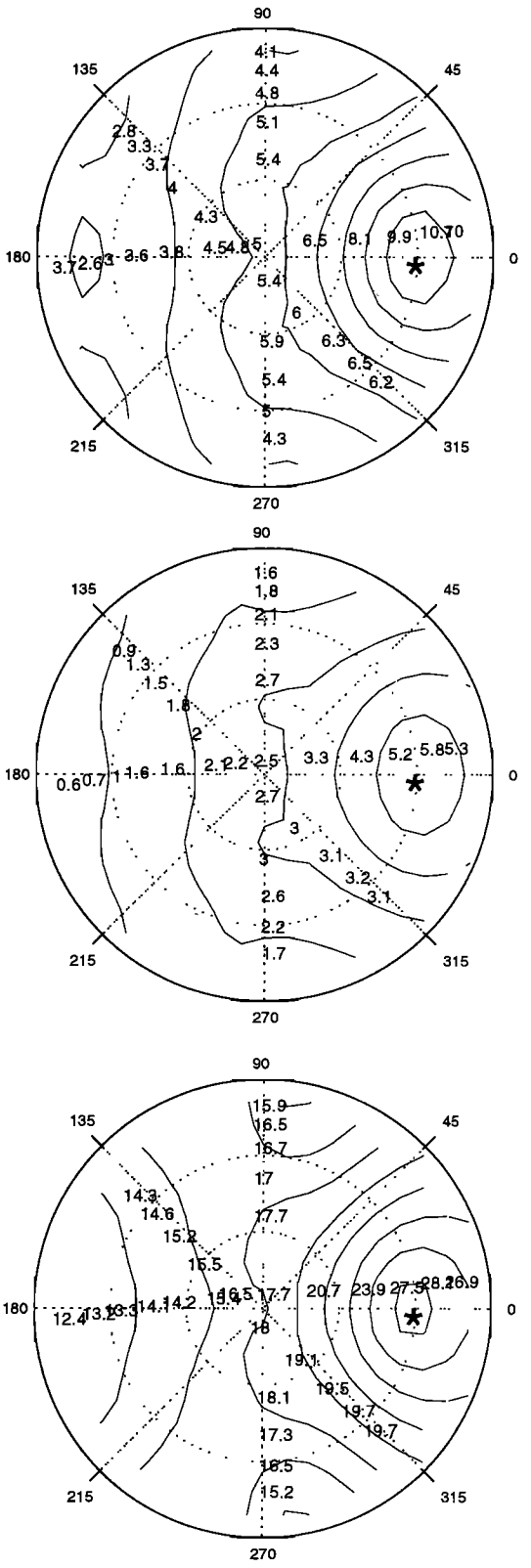

Figure 2. Same as Figure 1 but for the old black spruce site on May 31.

670 nm, and 2 at 864 nm, whereas for the aspen stands, it was about 2 at 550 nm, 3 at 670 nm, and 1.5 at 864 nm.

The spectral dependence of this ratio may be explained by two effects. First, in the near infrared, multiple scattering generates a significant contribution to the signal. Since this contribution is less anisotropic than the single scattering one, it decreases the ratio of maximum to minimum reflectance. Second, the canopy did not completely cover the surface so the soil

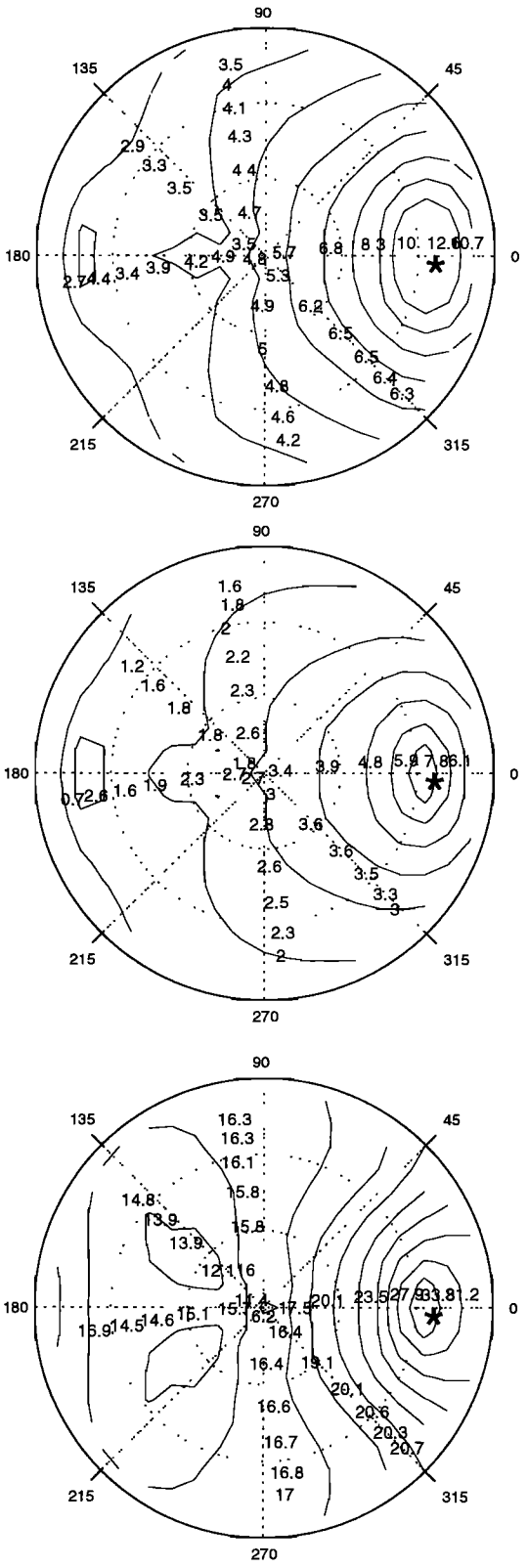

Figure 3. Same as Figure 1 but for the old jack pine site on May 31.

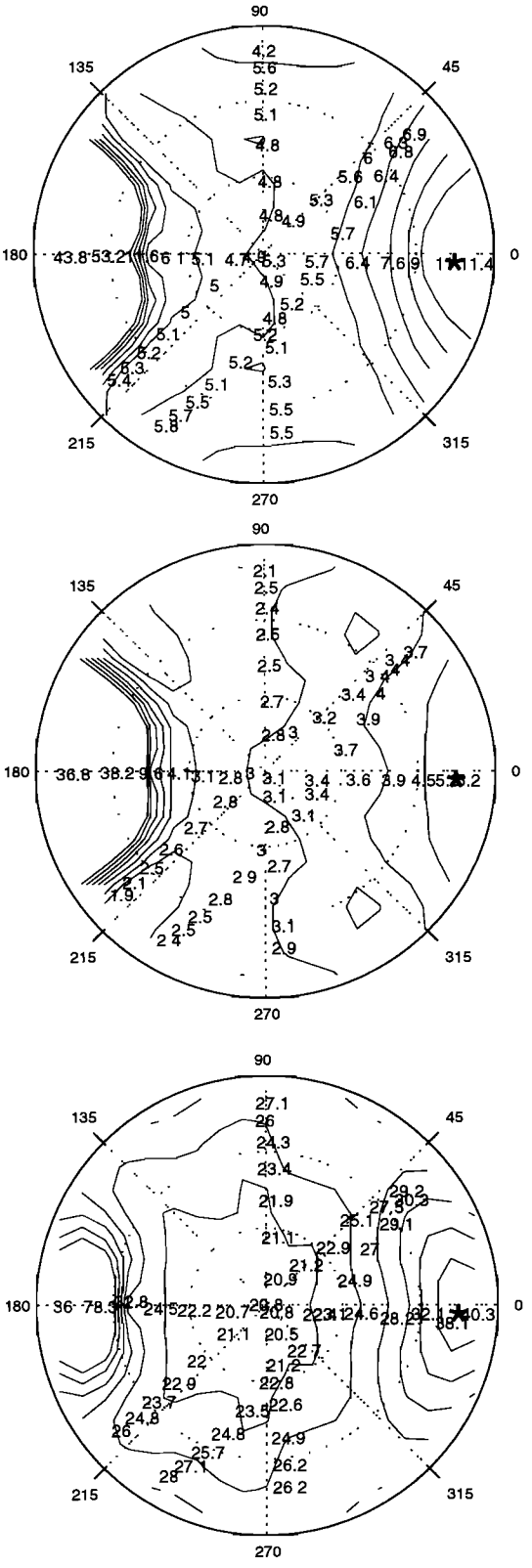

Figure 4. Same as Figure 1 but for the fen site on July 24.

contributed to the measured reflectance. The larger ratio observed at 670 nm, where leaf reflectance is lower, was probably due to the high contrast between leaf and soil reflectance at this wavelength and to the viewing of a large fraction of illuminated soil in the hot spot direction. This fraction was very small in the forward plane. The dependence with species of the ratio was expected, since the branch and leaf architecture of coniferous forests, and also their undergrowth, is quite different from those of deciduous forests.

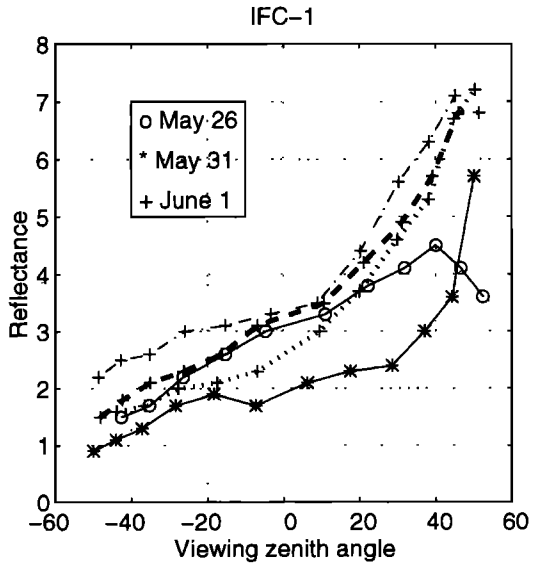

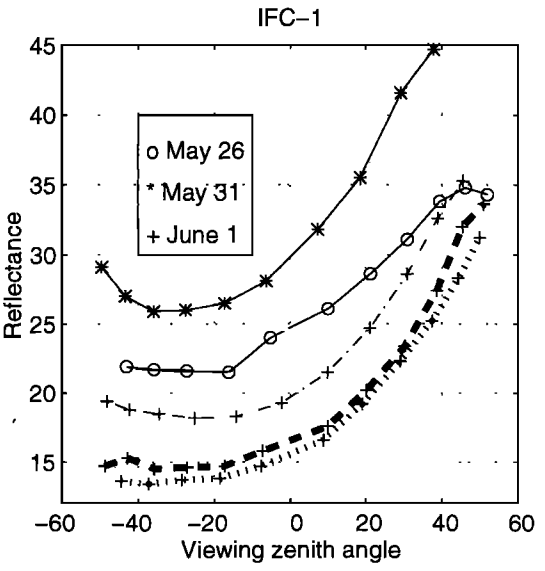

670 nm

864 nm

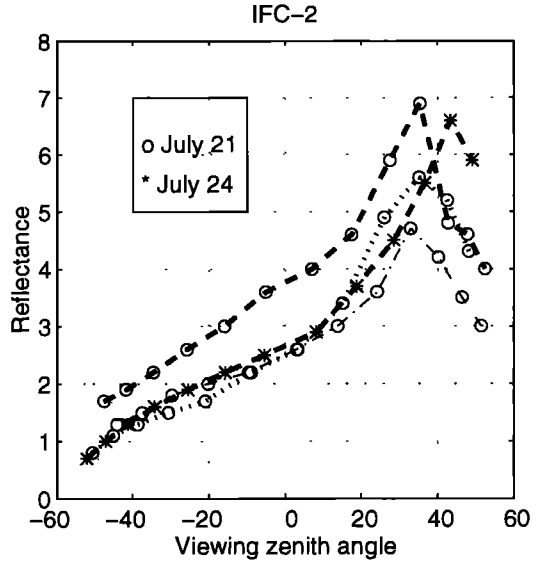

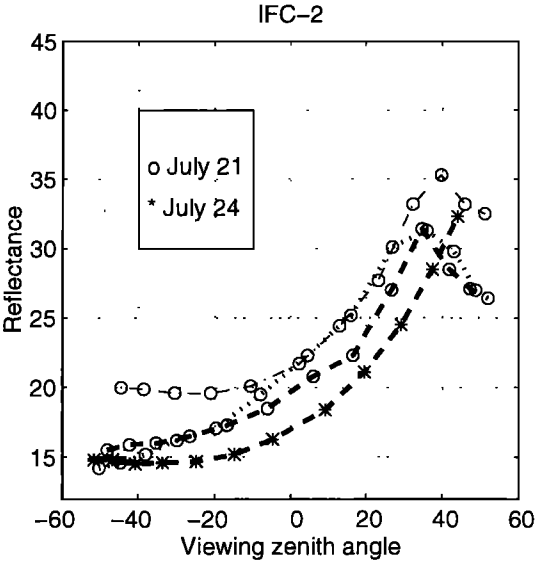

Figure 5. Reflectances at 670 nm in principal plane for old jack pine (thick dashed line), old aspen (solid line), young jack pine (dotted-dashed line), and old black spruce (dotted line) for several dates of IFC 1 (top) and IFC 2 (bottom), corrected for atmospheric effects.

Figure 6. Same as Figure 5 but at 864 nm.

The directional signature of the fen (Figure 4) contained an energetic component near the specular direction and was thus quite distinct from the signatures shown above. The fen surface consisted of high grasses imbedded in water, which gave rise to the specular signature. The amplitude of the specular signal, 43.8% at 550 nm, 38.2% at 670 nm, and 78.3% at 864 nm, was considerably larger than the local maximum observed in the hot-spot direction. These high values were obtained because the viewing zenith angle was very close to the Sun zenith angle ($\theta_v = 45.0°$, $\theta_s = 45.8°$, and $\phi = 180.5°$ at 550 nm). Other than this particular measure, the general shape of the signature was similar to the preceding signatures. Quite interestingly, the fen reflectance observed at nadir had a spectral signature similar to that of grasslands. This is because the underlying water, partially hidden by grasses, has at nadir a very low reflectance.

To emphasize the dependences of the data upon time, wavelength, and species, the reflectances in the principal plane of the entire data set of Table 1, with exception of the fen data, are displayed in Figures 5–7. Figures 5 and 6 regroup data per wavelength (670 and 864 nm) and per intensive field period (IFC 1 and IFC 2). Figure 7 compares data at two different periods, for the only data having similar Sun zenith angles in the two periods, that is, for the old black spruce and old jack pine sites.

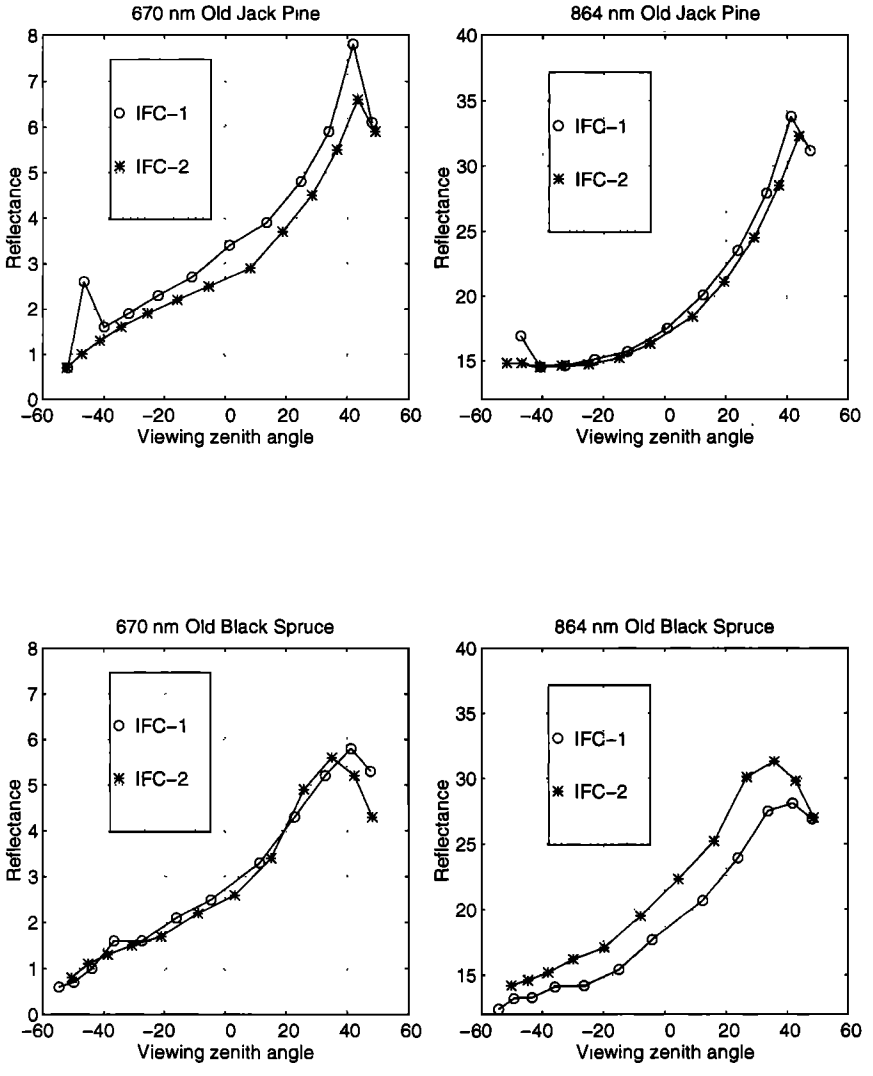

Figure 7. Comparison of principal planes acquired in IFC 1 and IFC 2 for old black spruce and old jack pine, at 670 nm and 864 nm.

The general patterns shown in Figures 5–7 support statements presented earlier on the shape of the BRDF, and the mentioned differences of spectral signatures between aspen and conifer stands. These figures also show the following. (1) The diurnal variations of reflectance were in some occasions very high, probably as a consequence of changes of Sun position. For example, the old aspen reflectance changed considerably within just 5 days (see top of Figures 5 and 6), while the Sun angle varied from 39° to 50° between the two data sets. Likewise, the old jack pine reflectance changed significantly between July 21 and 24, with corresponding variations of the Sun angle from 35° to 42° (bottom of Figures 5 and 6). By contrast, Figure 7 shows that when the Sun angle remained nearly constant, the reflectance of conifer stands changed only slightly from late spring to early summer. This is not surprising, since the seasonal variations of biophysical parameters of conifer stands, especially leaf area index, are expected to be small. (2) The hot spot feature was wider at 864 nm (Figure 6) than at 670 nm (Figure 5), as noted and commented by *Bréon et al.* [1997]. This width had some variability with species, more at 864 nm than at 670 nm; it was larger for black spruce stands than for jack pine stands. This variation could be explained by differences of internal crown structure and tree density in the two cases.

5. Enhanced Discrimination of Various Forest Covers Using Their Directional Signature

The results of the previous section suggest that information specific to forest cover species is contained in the directional signature and that discrimination of forest covers should be enhanced if directional information is added to the spectral information. In this section we attempt to quantify the degree to which this statement is true.

5.1. Experimental Protocol

The principle of the method is to compare the efficiency of supervised classifications with and without directional information. To quantify this information, one adjusts the BRDF of several tens of surface targets, corresponding to various cover types, against a three-parameter BRDF model. Then the reflectances in three given viewing directions and three spectral bands (centered on 550, 670, and 864 nm) are reconstructed using the model. This data set (three spectral bands, three

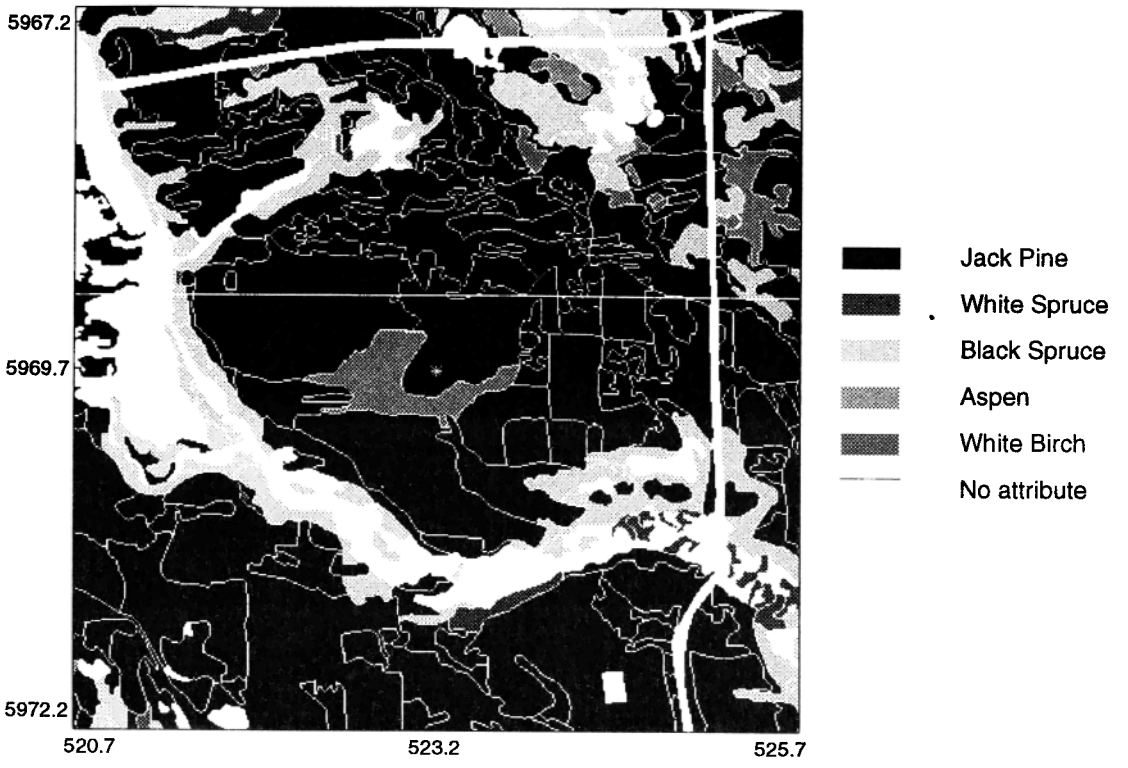

Figure 8. Map of primary species for an area 5 km × 5 km surrounding the young jack pine site.

directions, for each surface target) is used in multispectral classifications considering either three or one direction per spectral band and per pixel, and in monospectral classifications with either three or one direction per pixel. The method is described in more detail below.

From the POLDER data acquired on July 21, 1994, a BRDF was extracted on each 100-m resolution grid pixel of two large areas surrounding the young jack pine and old black spruce tower sites, and then corrected for atmospheric effects (section 3). The number of directional measurements associated with each pixel depends on the pixel position in the study area and on the number of flight axes. It equals about 40 at the center of the area and decreases slightly toward its corners. For each pixel the BRDF measurements acquired by POLDER are adjusted against the three-parameter semiempirical model of *Rahman et al.* [1993], shown below as (1):

$$\rho(\theta_s, \theta_v, \phi) = \rho_0 P(g)[1 + R(G)] \frac{\cos^{k-1} \theta_v \cos^{k-1} \theta_s}{(\cos \theta_s + \cos \theta_v)^{1-k}} \quad (1)$$

where $\rho(\theta_s, \theta_v, \phi)$ is the surface bidirectional reflectance and ρ_0 and k are empirical parameters. The term $P(g)$ represents the average phase function of the scatterers:

$$P(g) = \frac{1 - \Theta^2}{[1 + \Theta^2 - 2\Theta \cos(\pi - g)]^{1.5}} \quad (2)$$

where Θ is the asymmetry factor, ranging from -1 to $+1$. The phase angle g is defined by

$$\cos g = \cos \theta_v \cos \theta_s + \sin \theta_v \sin \theta_s \cos \phi \quad (3)$$

The hot-spot effect is approximated by the function $R(G) = (1 - \rho_0)/(1 + G)$, where G is a geometry factor given by $G = (\tan^2 \theta_v + \tan^2 \theta_s - 2 \tan \theta_v \tan \theta_s \cos \phi)^{0.5}$. From the parameters ρ_0, k, and Θ retrieved through the adjustment between model and observations, the reflectance of each 100 m × 100 m pixel is reconstructed in three different viewing directions (and the same Sun zenith angle as in the original data set): nadir, hot spot, and in the perpendicular plane for $\theta_v = 50°$.

We used subsets of forest cover georeferenced maps, available in the BORIS database, covering the same 5 km × 5 km areas mentioned above. These maps describe various canopy attributes such as density, height, and primary, secondary, and tertiary species. They were derived by photointerpretation of near-infrared aerial photography with field reconnaissance notes. As an illustration, the map of the primary species at the original resolution for the young jack pine area is shown in Figure 8. The format and resolution of these maps were made compatible with those of the BRDF to be able to compare both types of information. On the basis of the land cover maps, we selected five different classes of forest covers, named black spruce (BS), jack pine small (JPs), jack pine tall (JPt), aspen (A), and white spruce (WS), the attributes of which are described in Table 3. The selection was made according to several criteria. First, the number of pixels with the same attributes must be as large as possible for statistical significance. Second, the class attributes must be sufficiently distinct from each other. Third, a pixel was retained in a class if the correlation coefficient of the adjustment between model and observations was larger than 0.9. This process yielded 30 selected pixels per class.

The results of a supervised classification on all selected pixels were then compared, using as input either reflectances at nadir only (this simulates the case of conventional remote sensing measurements) or reflectances reconstructed in the

Table 3. Forest Cover Classes With Their Respective Attributes

Class Symbol	Primary Species	Density, %	Height, m	Secondary Species	Tertiary Species
BS	black spruce (*Picea mariana*)	>80	7.5–12.5		
JP_s	jack pine (*Pinus banksania*)	55–80	2.5–7.5	aspen	
JP_t	jack pine (*Pinus banksania*)	>80	17.5–22.5		
A	aspen (*Populus tremoloides*)	55–80	>22.5		white spruce
WS	white spruce (*Picea glauca*)	55–80	>22.5	aspen	

three directions mentioned above (this simulates the case where directional signatures are also accounted for). The number N of dimensions may be 1 (one spectral band, one direction), 3 (three spectral bands, one direction or three directions, one spectral band), or 9 (three directions, three spectral bands). For each of the five classes j, the N-dimensional vector M_j, representing the average of the N-dimensional reflectances x in class j, and the $N \times N$ covariance matrix Q_j were computed for each classification experiment. The classification was made using a standard criterion of maximum likelihood. The density of probability $P(x \in C_j)$ that a pixel x belongs to class C_j was calculated using the formula

$$P(x \in C_j) = \frac{1}{\sqrt{(2.\pi)^N |Q_j|}} \exp\left[-\tfrac{1}{2}(x - M_j)' Q_j^{-1}(x - M_j)\right] \quad (4)$$

where $|Q_j|$ is the determinant of Q_j. The supervised classification affected each pixel to the class j for which the probability $P(x \in C_j)$ was maximum. The classification efficiency was quantified by the confusion matrix C_{ij}, which describes the number of pixels belonging to class C_i which are affected to class C_j.

5.2. Results

The first step of the analysis is to evaluate the amount of additional information in the directional signature. There was no distinction at this stage between training and test pixels. The confusion matrix in multidirectional and monospectral space (three dimensions) was compared to that in monodirectional (nadir) and monospectral space (one dimension) in Table 4 at 550, 670, and 864 nm. The results show that forest species discrimination was enhanced greatly when directional information was added to the monospectral information. In monodirectional and monospectral space the proportion of correctly classified pixels was 49%, 55%, and 59% for 550, 670, and 864, respectively. These values improved to 81%, 77%, and 84% in multidirectional and monospectral space. Many off-diagonal matrix coefficients approached zero in multidirectional space (Table 4). However, the confusion was high for the Aspen class both in three-dimensional and one-dimensional space, and

Table 4. Confusion Matrix C_{ij} in the Case of Multidirectional and Monospectral Space, and in the Case of Monodirectional and Monospectral Space, at 550, 670, and 864 nm

	Monodirectional and Monospectral Space					Multidirectional and Monospectral Space				
Class	BS	JP_s	JP_t	A	WS	BS	JP_s	JP_t	A	WS
					*550-nm Channel**					
BS	21	0	4	0	5	29	0	0	1	0
JP_s	0	25	5	0	0	0	26	4	0	0
JP_t	17	9	3	0	1	0	2	27	1	0
A	4	5	2	0	19	0	3	2	12	13
WS	6	0	0	0	24	0	0	0	2	28
					670-nm Channel†					
BS	24	0	3	0	3	27	0	0	2	1
JP_s	0	27	3	0	0	0	27	0	3	0
JP_t	21	4	4	0	1	0	4	26	0	0
A	4	6	2	0	18	0	4	0	8	18
WS	1	0	1	0	28	1	0	0	2	27
					864-nm Channel‡					
BS	28	1	0	0	1	25	1	0	0	4
JP_s	0	27	0	2	1	0	30	0	0	0
JP_t	1	6	0	13	10	1	0	20	3	6
A	0	10	1	18	1	1	0	3	26	0
WS	10	3	0	1	16	1	0	2	2	25

The term C_{ij} describes the number of pixels belonging to class C_i which are affected in class C_j. Also indicated is the percentage of correctly classified pixels, which is the sum of the diagonal elements of C_{ij} divided by the total number of pixels (150).

*Percentage of correctly classified pixels is 48.6% in monodirectional and monospectral space and 81.3% in multidirectional and monospectral space.

†Percentage of correctly classified pixels is 55.3% in monodirectional and monospectral space and 76.6% in multidirectional and monospectral space.

‡Percentage of correctly classified pixels is 59.3% in monodirectional and monospectral space and 84.0% in multidirectional and monospectral space.

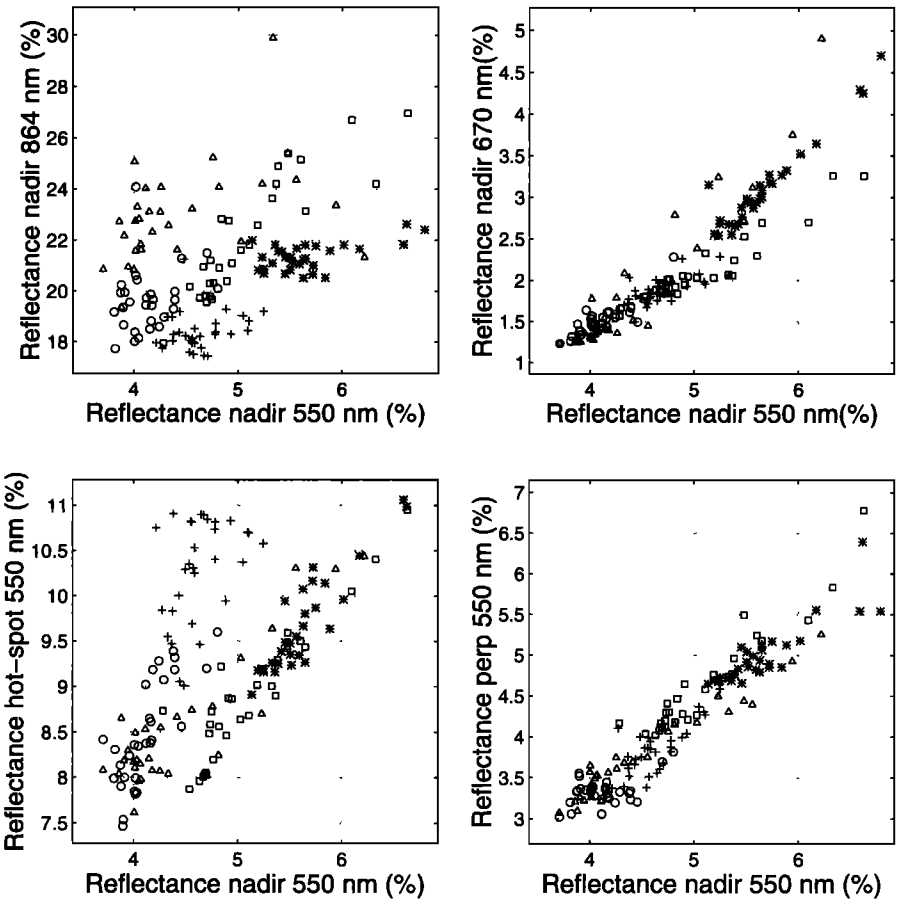

Figure 9. Class representation. (top) Nadir reflectances at 864 nm (left) and 670 nm (right) versus 550 nm (bottom). The 550 nm reflectances for hot spot (left) and perpendicular plane at 50° viewing angle (right), versus nadir. Cross, black spruce; star, jack pine small; square, jack pine tall; triangle, aspen; circle, white spruce.

many Aspen pixels were classified in the white spruce class. This could be explained by the similarity of aspen and white spruce class attributes, since their density and height were in fact the same. Moreover, the nondominant species of the aspen class was the primary species of the white spruce class (Table 3).

Using this data set, one can determine whether it is preferable to operate a sensor with multidirectional capability with only one spectral band (and then, which one), or a sensor with multispectral capability at only one view direction. Figure 9 represents the repartition of the 150 pixels in a specific case, three wavelengths at nadir, versus three directions at 550 nm. This figure illustrates that the two situations have apparently equivalent discriminative capabilities. A quantitative evaluation is given by Table 5, which displays elements of the confusion matrix in monodirectional and multispectral space (three dimensions) according to the three directions, for comparison with the results of Table 4. The proportion of correctly classified pixels was 86%, 81%, and 84% for the nadir direction, the hot spot direction, and the direction in the perpendicular plane for $\theta_v = 50°$, respectively. These results are slightly higher than those obtained in multidirectional and monospectral space for the three wavelengths (76–84%; see above). Information in Table 5 suggests that land cover discrimination will be slightly better with multispectral sensors with one view direction, than with multidirectional sensors with only one spectral band.

It is also possible to compare situations where three spectral bands are available with only one direction (three dimensions), and where three spectral bands are available with three directions per spectral band (nine dimensions). The improvement of class discrimination was then significant, as shown in Table 6. The percentage of correctly classified pixels increases from 80–86% (three dimensions) to 97% (nine dimensions). Only a few aspen pixels were incorrectly affected to the white spruce class in this latter case. The confusion was much smaller when all directions and spectral bands were taken into account than when only spectral information was considered.

The second step of the analysis is to derive a performance level of supervised classifications which make use of directional channels. It is necessary at this stage to separate training and test pixels. We performed a series of 10 numerical experiments similar to those described above using 15 training pixels and 15 test pixels for each class. The small number of elements per class in this case can only lead to an approximate prediction of supervised classification performances. The range of correctly classified test pixels in the 10 experiments was 36–59% in monodirectional, monospectral space, 64–81% in multidirectional, monospectral space, 72–87% in monodirectional, multispectral space, and 83–91% in multidirectional, multispectral space. The dispersion of results in the various experiments was high, as expected given the small number of test pixels. The performance levels were logically lower than above, since we used separate sets of training and test pixels. Nevertheless, the

Table 5. Same as Table 4 in the Case of Monodirectional and Multispectral Space for Three Viewing Directions

Direction	Class	Monodirectional and Multispectral Space				
		BS	JP_s	JP_t	A	WS
Nadir*	BS	26	0	1	0	3
	JP_s	0	29	0	1	0
	JP_t	3	0	26	1	0
	A	0	1	1	22	6
	WS	0	1	2	1	26
Hot spot†	BS	26	2	1	1	0
	JP_s	0	26	3	1	0
	JP_t	0	0	18	1	11
	A	0	1	1	26	2
	WS	1	1	2	1	25
Perpendicular plane‡	BS	25	0	2	1	2
	JP_s	0	26	3	1	0
	JP_t	1	0	29	0	0
	A	2	1	0	19	8
	WS	1	0	0	2	27

*Percentage of correctly classified pixels is 86%.
†Percentage of correctly classified pixels is 80.6%.
‡Percentage of correctly classified pixels is 84.0%.

results confirm the importance of directional information and provide an approximate prediction of the performance of supervised classifications using spectral or directional information, or both.

6. Conclusion

The study describes the anisotropy of reflectance signatures of various types of forest covers measured by the airborne POLDER instrument during the BOREAS experiment. The process included (1) calibration using several cross-checked calibration experiments, (2) atmospheric corrections, using as input atmospheric aerosol thickness measurements acquired during flight, and (3) geometric corrections, using onboard navigation data and fine multi-image registration with ground control point techniques.

Several examples of directional and spectral signatures were documented (1) over coniferous forests at the young jack pine, old jack pine, and old black spruce sites, (2) over a deciduous forest at the old aspen site, and (3) over a fen at the fen site. All signatures were found to be highly anisotropic, primarily along the principal solar plane, with only slight variations in the perpendicular plane. The hot-spot reflectance peak occurring when Sun and view directions coincide, was quite apparent at all wavelengths, with a ratio of maximum to minimum reflectance in the principal plane of the order of 4–8 in the visible and 1.5–2 in the near infrared. The directional signature of the fen showed an energetic component in the specular direction and was thus quite distinct from the signatures of forests. When observed at nadir, the fen had a spectral reflectance near that of grasslands and, consequently, cannot be identified as a fen from observations that deviate very far from the specular direction. These results support the idea, first suggested by Vanderbilt [*Vanderbilt et al.*, 1997], that observations made in the specular direction hold great promise for the mapping and characterization of fen areas. The analysis of directional signatures of various forest covers at different times of observation showed that the directional content provides an important source of information, which can enhance the discrimination of forest types.

Table 6. Same as Table 4 in the Case of Multidirectional and Multispectral Space

Class	Multidirectional and Multispectral Space				
	BS	JP_s	JP_t	A	WS
BS	30	0	0	0	0
JP_s	0	30	0	0	0
JP_t	0	0	30	0	0
A	0	0	0	26	4
WS	0	0	0	1	29

Percentage of correctly classified pixels is 96.6%.

A key objective of this study was to quantify, using a supervised classification procedure, the improvement of forest cover discrimination through use of the directional signature in addition to the more usual spectral information. The experiment consisted in the selection of five sufficiently distinct classes in terms of species and tree heights, with digital forest cover maps, and of 30 pixels per class, with POLDER BRDF data sets covering two areas of size 5 km × 5 km at resolution 100 m × 100 m. The use of a bidirectional reflectance model adjusted against the directional measurements allowed for each pixel to reconstruct reflectances in three different directions (hot-spot, nadir, and in the perpendicular plane for a viewing zenith angle of 50°) at three wavelengths centered on 550, 670, and 864 nm. When only one wavelength was used, the results showed that in multidirectional space (three dimensions), the proportion of correctly classified pixels was much higher than in monodirectional space. This proportion was also significantly higher in multidirectional, multispectral space (nine dimensions), than in monodirectional, multispectral space (three dimensions). We conclude that the account of directional information enhances the ability to discriminate forest covers by remote sensing. Besides, if only three channels of information were available, it seems slightly preferable to use three different spectral bands and one direction of observation, rather than three directions of observation with one spectral band.

The land cover classification method outlined in this paper can be applied to the data from present and future spaceborne

instruments with directional capability, such as POLDER, recently launched on the Japanese ADEOS platform, and multiangle imaging scanning radiometer (MISR), which will be launched shortly on the U.S. EOS platform. This will permit an analysis of the information content of reflectance directional signatures for the characterization and discrimination of continental surfaces at regional and global scales.

Acknowledgments. The airborne POLDER instrument was built by Laboratoire d'Optique Atmosphérique (LOA) of Lille, with sponsorship from Centre National d'Etudes Spatiales (CNES). It was kindly provided to us by LOA. We acknowledge the work of J. Y. Balois (LOA), who performed the calibration of the instrument. We are also indebted to J. Schaffer and B. Markham (NASA Goddard), who performed an instrument calibration during the BOREAS experiment. We thank the air crews of the NASA C-130 for their excellent support. The original data for forest cover maps were acquired by Saskatchewan Environment and Resource Management, Forestry Branch–Inventory Unit (Prince Albert), while the associated vector data were processed and gridded by the BOREAS Information System staff (NASA Goddard). We thank J. Benson, F. Gruska (Prince Albert), B. McCowan, and J. Nickeson (NASA Goddard) for providing help and assistance regarding these data. This study was funded by Programme National de Télédétection Spatiale (PNTS) and Région Midi-Pyrénées.

References

Abuelgasim, A. A., S. Gopal, J. R. Irons, and A. H. Strahler, Classification of ASAS multiangle and multispectral measurements using artificial neural networks, *Remote Sens. Environ.*, *57*, 79–87, 1996.

Achard, F., and C. Estreguil, Forest classification of southern Asia using NOAA AVHRR data, *Remote Sens. Environ.*, *54*, 198–208, 1995.

Bréon, F. M., V. Vanderbilt, M. Leroy, P. Bicheron, C. L. Walthall, and J. E. Kalshoven, Evidence of hot-spot signature from airborne POLDER measurements, *IEEE Trans. Geosci. Remote Sens.*, **35**, 479–484, 1997.

Deering, D. W., E. M. Middleton, and T. F. Eck, Reflectance anisotropy for a spruce-hemlock forest canopy, *Remote Sens. Environ.*, *47*, 242–260, 1994.

Deschamps, P. Y., F. M. Bréon, M. Leroy, A. Podaire, A. Bricaud, J. C. Buriez, G. Sèze, The POLDER mission: Instrument characteristics and scientific objectives, *IEEE Trans. Geosci. Remote Sens.*, *32*, 598–615, 1994.

Goel, N. S., and N. E. Reynolds, Bidirectional canopy reflectance and its relationship to vegetation characteristics, *Int. J. Remote Sens.*, *10*, 107–132, 1989.

Gutman, G. G., The derivation of vegetation indices from AVHRR data, *Int. J. Remote Sens.*, *8*, 1235–1243, 1987.

Hyman, A. H., and M. J. Barnsley, On the potential for land-cover mapping from multiple-view angle (MVA) remotely sensed images, *Int. J. Remote Sens. Lett.*, in press, 1997.

Irons, J. R., K. J. Ranson, D. L. Williams, R. R. Irish, and F. G. Huegel, An off-nadir pointing imaging spectroradiometer for terrestrial ecosystem studies, *IEEE Trans. Geosci. Remote Sens.*, *29*, 66–74, 1991.

Kimes, D. S., Dynamics of directional reflectance factor distributions for vegetation canopies, *Appl. Opt.*, *22*, 1364–1373, 1983.

Kimes, D. S., W. W. Newcomb, R. F. Nelson, and J. B. Schutt, Directional reflectance distributions of a hardwood and pine forest canopy, *IEEE Trans. Geosci. Remote Sens.*, *GE-24*, 281–293, 1986.

Kleman, J., Directional reflectance factor distributions for two forest canopies, *Remote Sens. Environ.*, *23*, 83–96, 1987.

Kuusk, A., Determination of vegetation canopy parameters from optical measurements, *Remote Sens. Environ.*, *37*, 207–218, 1991.

Leroy, M., and F. M. Bréon, Surface reflectance angular signatures from airborne POLDER data, *Remote Sens. Environ.*, *57*, 97–107, 1996.

Leroy, M., and J. L. Roujean, Sun and view angle corrections on reflectances derived from NOAA/AVHRR data, *IEEE Trans. Geosci. Remote Sens.*, *32*, 684–696, 1994.

Markham, B. L., D. L. Williams, J. R. Schaffer, F. Wood, and M. S. Kim, Radiometric characterization of diode-array field spectroradiometers, *Remote Sens. Environ.*, *51*, 317–330, 1995.

Morton, A. J., Moorland plant community recognition using Landsat MSS data, *Remote Sens. Environ.*, *20*, 291–298, 1986.

Rahman, H., B. Pinty, and M. M. Verstraete, A coupled surface atmosphere reflectance (CSAR) model, 2, A semi-empirical model useable with NOAA/AVHRR data, *J. Geophys. Res.*, *98*, 20,791–20,801, 1993.

Ranson, K. J., C. S. T. Daughtry, and L. L. Biehl, Sun angle, view angle, and background effects on spectral response of simulated balsam fir canopies, *Photogramm. Eng. Remote Sens.*, *52*, 649–658, 1986.

Roujean, J. L., M. Leroy, A. Podaire, and P. Y. Deschamps, Evidence of surface reflectance bidirectional effects from a NOAA/AVHRR multi-temporal dataset, *Int. J. Remote Sens.*, *13*, 685–698, 1992.

Russell, C. A., C. L. Walthall, J. R. Irons, and E. C. Brown de Colstoun, Comparison of airborne and surface spectral bidirectional reflectance factors, spectral hemispherical reflectance, and spectral vegetation indices, *J. Geophys. Res.*, *100*, 25,509–25,522, 1995.

Schaaf, C. B., and A. H. Strahler, Validation of bidirectional and hemispherical reflectances from a geometric-optical model using ASAS imagery and pyranometer measurements of a spruce forest, *Remote Sens. Environ.*, *49*, 138–144, 1994.

Sellers, P. J., C. J. Tucker, G. J. Collatz, S. O. Los, C. O. Justice, D. A. Dazlich, and D. A. Randall, A global 1 × 1 degree dataset for climate studies, 2, The generation of global fields of terrestrial biophysical parameters from the NDVI, *Int. J. Remote Sens.*, *15*, 3519–3545, 1994.

Singh, A., Spectral separability of tropical forest cover classes, *Int. J. Remote Sens.*, *8*, 971–979, 1987.

Syrén, P., Reflectance anisotropy for nadir observations of coniferous forest canopies, *Remote Sens. Environ.*, *49*, 72–80, 1994.

Townshend, J. R. G., C. O. Justice, and V. T. Kalb, Characterization and classification of South American land cover types using satellite data, *Int. J. Remote Sens.*, *8*, 1189–1207, 1987.

Tucker, C. J., J. R. G. Townshend, and T. E. Goff, African land classification using satellite data, *Science*, *227*, 369–375, 1985.

Vanderbilt, V. C., et al., Discrimination of wetland and non-wetland community types with multi-spectral, multi-angle, polarized POLDER data, in *Seventh International Symposium on Physical Measurements and Signatures in Remote Sensing, Courchevel*, Int. Soc. for Photogramm. and Remote Sens., 1997.

Vermote, E., D. Tanré, J. L. Deuzé, and J. J. Morcrette, Second simulation of the satellite signal in the solar spectrum: An overview, *IEEE Trans. Geosci. Remote Sens.*, in press, 1997.

Walker, J., D. L. B. Jupp, L. K. Penridge, and G. Tian, Interpretation of vegetation structure in Landsat MSS imagery: A case study in disturbed semiarid eucalyptwoodlands, 1, Field data analysis, *J. Environ. Manage.*, *23*, 19–35, 1986.

Wu, A., Z. Li, and J. Cihlar, Effects of land cover type and greeness on advanced very high resolution radiometer bidirectional reflectances analysis and removal, *J. Geophys. Res.*, *100*, 9179–9192, 1995.

P. Bicheron, O. Hautecoeur, and M. Leroy, Centre d'Etudes Spatiales de la Biosphère, UMR CNES-CNRS-UPS, 18 Avenue E. Belin, 31401 Toulouse Cedex, France. (e-mail: marc.leroy@cesbio.cnes.fr)

F. M. Bréon, Laboratoire de Modélisation du Climat et de l'Environnement, CEA/DSM/LMCE, 91191 Gif sur Yvette Cedex, France.

(Received September 30, 1996; revised April 28, 1997; accepted May 2, 1997.)